# Double Passive Cavitation Detection of Optison™ Shell Rupture

Azzdine Y. Ammi[1], Robin O. Cleveland[2], Jonathan Mamou[3], Grace I. Wang[3], S. Lori Bridal[1], William D. O'Brien, Jr.[3];
[1]Laboratoire d'Imagerie Paramétrique, UMR 7623 C.N.R.S, 15 rue de l'école de médecine, 75006 Paris, France (bridal@lip.bhdc.jussieu.fr); [2]Department of Aerospace and Mechanical Engineering, Boston University, Boston, MA 02215;
[3]Bioacoustics Research Laboratory, Department of Electrical and Computer Engineering, University of Illinois at Urbana-Champaign, Urbana, IL 61801.

***Abstract*—An improved understanding of ultrasound contrast agent (UCA) shell rupture is required to optimize therapeutic and diagnostic use. This experimental and theoretical study aims to explore the mechanism of UCA shell rupture by determining thresholds as a function of ultrasonic excitation parameters (driving frequency, pulse duration, and peak rarefactional pressure). The experimental setup is based on a passive cavitation detection system described in previous work. However, this system has been modified to allow simultaneous acquisition of the signals received with the 13-MHz passive receiver and the signals incident upon the lower frequency (0.9, 2.8 and 4.6 MHz) transmitting transducer functioning in the pulse-echo mode. Post-excitation signals were used to detect rupture thresholds. By allowing acquisition of the signals received by the insonifying transducer (pulse-echo during the excitation and passively at post-excitation) additional information is obtained within a frequency range and a transmission/reception configuration typical of ultrasonic diagnostic imaging. Data are analyzed to estimates the incident peak rarefactional pressure leading to 50% destruction. Comparison of experimental results with microbubble dynamics predicted using the Modified Herring equation was used to explore microbubble rupture indices based on radial expansion and peak velocity.**

## I. Introduction

By causing local ultrasound contrast agent (UCA) destruction in a selected region to purposefully modify UCA concentration, dynamic evaluation of image contrast-enhancement can be used to assess blood volume and flow rate [1,2]. However, UCA-based blood perfusion assessment is hampered by unintentional modification of UCA concentration during imaging and the unknown ultrasound backscattered echo contribution to the received signal by microbubble destruction. Knowledge of the UCA destruction thresholds is thus essential to develop quantitative perfusion imaging techniques. An understanding of microbubble destruction is also fundamental for the development of targeted contrast microbubbles carrying encapsulated medicines to a site for delivery initiated by ultrasonic capsule destruction [3,4].

In previous work using a passive cavitation detection (PCD) system [5] we demonstrated that post-excitation signals are linked to inertial cavitation (IC) and rebound events. The previous PCD study provided information concerning the rupture response only at relatively high frequencies (9 to 17 MHz). The current study extends this work by capturing simultaneously the signals received by the lower-frequency transmitting transducer. The lower-frequency signal provides additional information related to event timing and rupture characteristics detectable in the frequency range typical of ultrasonic diagnostic imaging. Data analysis is performed to identify 50% destruction pressure thresholds. Comparison between experimental results and theoretical predictions is also performed to gain insight into the nature of the rupture thresholds.

## II. Materials and Methods

### *A. Double Passive Cavitation Detector (DPCD)*

The experimental setup is based on the PCD system described previously [5]. The experiments were carried out in a Plexiglas tank (50.5-cm long x 25.5-cm wide x 30.0-cm high), containing 19.2 ± 0.3 L of degassed water between 20 and 22°C. In addition to the acquisition of signals passively received by the 13-MHz transducer, the receive electronics were modified so that the signals incident upon the transmit transducer coinciding with (pulse-echo) and following (passive) the excitation could be acquired (Fig 1).

The effective -6-dB focal volume for the DPCD is limited by the -6-dB volume of the transmit transducer instead of that of the more highly focused receive transducer (estimations were made with a reflective wire [5]). It was thus necessary to reduce the mean concentration of UCAs injected into the tank relative to the concentrations used previously by the PCD system to ensure that, on average, only one UCA was within the effective volume at any given time.

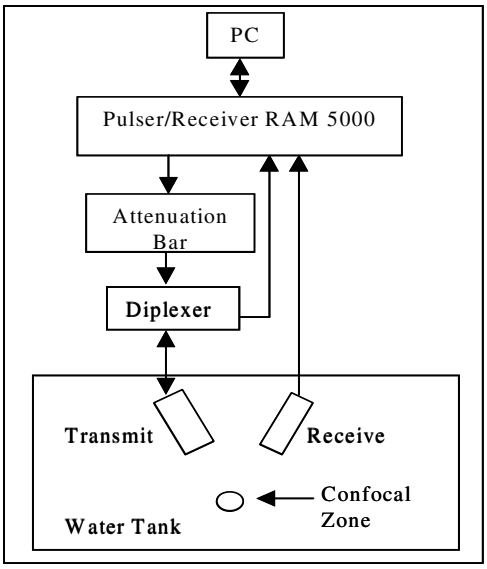


Figure 1. Diagram of the experimental system showing the transducer configuration and the associated electronics.

### B. Data acquisition

The output from the 13-MHz transducer was amplified by 44 dB and that from the transmit transducer by 22 dB. The data were digitized (12-bit, 100 MHz, Strategic Test digitizing board UF 3025, Cambridge, MA) and saved to a personal computer.

Prior to each series of data acquisitions, the tank was filled with degassed water. The focal region of the selected transmit transducer was aligned with that of the receiver. Using a graduated syringe, 0.1 mL of Optison™ was injected into the tank corresponding to approximately $0.5 \times 10^8$ microbubbles, and resulted in a mean concentration of about 2 microbubbles/μL. The water was gently stirred with a pump before and during data acquisition to maintain an even UCA distribution and to ensure its replenishment in the active volume. A 3-cycle pulse duration (PD) at the transmitter's center frequency was generated. For each transmit pressure amplitude (varied from highest to lowest), 128 consecutive received waveforms were acquired from both transducers. This acquisition procedure was repeated for 5-cycle PDs and then 7-cycle PDs.

### C. Theoretical Model

The microbubble dynamics were modeled using the shelled microbubble model described by Morgan et al [6]. The model employs the modified Herring equation for microbubble dynamics with two additional terms to account for the elasticity and viscosity of the shell. The microbubble radius used in simulations was 2 μm and the shell thickness was 15 nm, which correspond to the mean values reported for Optison™ [7]. The shell elasticity was 4 N/m and the shell viscosity was 0.73 Pa.s. The incident acoustic waveforms measured with a calibrated hydrophone were used as the input acoustic driving pressures to the microbubble dynamics model.

## III. Results

### A. Minimum Thresholds for Rupture

Estimations of the pressure rupture thresholds were made based on the lowest peak rarefactional pressure that yielded post-excitation signals in any of the 128 waveforms acquired by the 13-MHz transducer. Results were consistent with those obtained previously [5] in terms of the general variation of the thresholds with frequency, pulse duration and pressure.

### B. Simultaneous waveforms

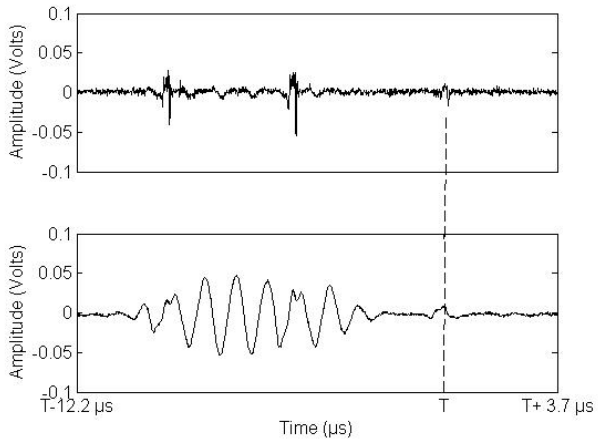


Figure 2. DPCD signals received for a 0.9-MHz, 7-cycle, 1.3 MPa excitation pulse. Top panel: Signal received with the 13-MHz transducer. Bottom Panel: Signal simultaneously received with the 0.9-MHz transducer. To adjust simultaneously occurring signals for differences in the transmit-receive paths, alignment was based on time-shifts to post-excitation peaks (T).

Fig 2 shows example time traces of the DPCD signals for 0.9-MHz excitation. The 13-MHz passive detection signal presents large-bandwidth peaks at several times during the excitation. The signal acquired with the 0.9-MHz transducer contains a pulse-echo response during excitation and evidence of a post-excitation response. Changes in the shape of the 0.9-MHz receive waveform coincide with the peaks in the 13-MHz signal. These waveforms are typical of those observed for 0.9-MHz excitation when post-excitation signals were present. When no post-excitation signals were present, no detectable peaks were observed with the 13-MHz receiver for 0.9-MHz excitation. At higher transmit frequencies (2.8 and 4.6 MHz) bubble oscillation is evident on waveforms received at 13 MHz.

### C. Percent destruction of microbubbles

An automatic detection of IC signals was applied to each set of 128 signals detected by the 13-MHz transducer to estimate the percent with rupture. This analysis was performed on the initial data set obtained with the PCD due to the fact that the number of microbubbles detected by the 13-MHz transducer with the DPCD system was quite small (because

the UCA was more diluted). Fig 3 shows the percentage of collapsing microbubbles as a function of excitation pressure for a 4.6-MHz 5-cycle excitation pulse. The 50% destruction level is reached at 2.5 MPa. Such curves were plotted for each set of incident pulse settings and fit to a logistic regression curve. Fig 4 summarizes the results for 50% destruction.

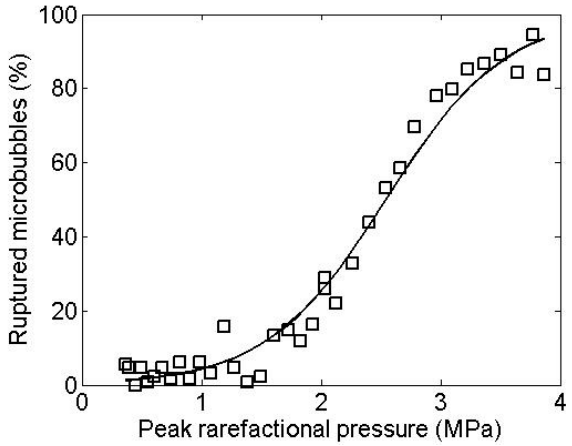


Figure 3 The squares represent the percent number of collapsed microbubbles at each incident pulse pressure for 4.6-MHz and 5-cycle excitation. The curve represents the logistic regression.

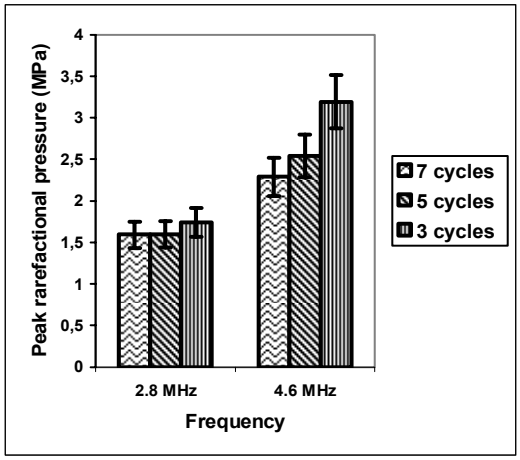


Figure 4. Peak rarefactional pressure thresholds yielding 50% destruction in Optison™. Error bars represent the estimated uncertainty in pressure measurement (10%). For curves describing the 0.9-MHz transducer response, the 50% destruction level was not reached for any of the studied PDs.

### *D. Evaluation of the response as a function of frequency*

For 5-cycle, 2.8- and 4.6-MHz incident pulses at pressures yielding 50% microbubble destruction, groups of 128 signals received at the transmit frequency and 13 MHz were classified as 1) presenting no evidence of a microbubble, 2) indicating an oscillation without collapse and 3) indicating collapse.

Then average spectra were compared for the groups of waveforms in class 2 and class 3. Spectra in Fig 6 (a) and (b) demonstrate additional broadband noise when bubble collapse was detected. Frequency components were similar with and without collapse.

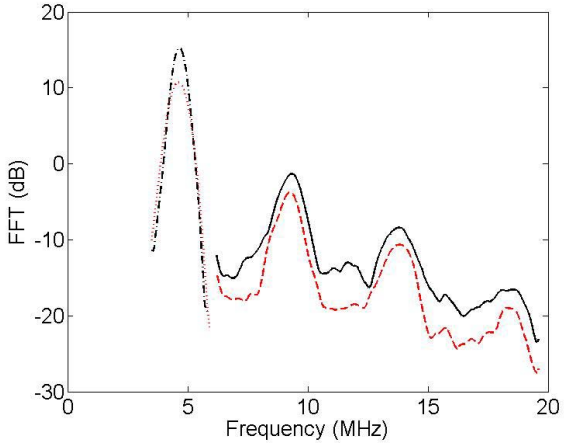


(a)

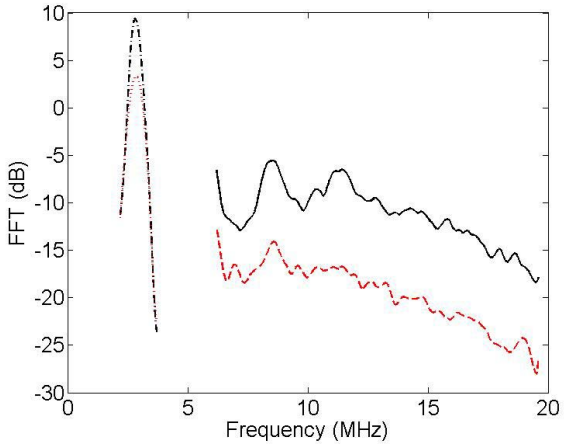


(b)

Figure 5 The black solid curves present the mean FFT from 13-MHz waveforms with IC. The dashed red curves present the mean FFT from 13-MHz waveforms without IC but with bubble oscillation during excitation. The dotted and dash-dotted curves present the mean FFT from waveforms acquired with the excitation transducer with and without evidence of IC, respectively. (a) Excitation at 4.6 MHz, 5 cycle, 2.5 MPa. (b) Excitation at 2.8 MHz, 5 cycle, 1.6 MPa.

### *E. Comparison between theory and experiment*

The relative radial expansion and peak velocity were calculated with the Herring model for each pulse duration and frequency at the rarefactional pressure yielding 50% destruction (Fig 7).

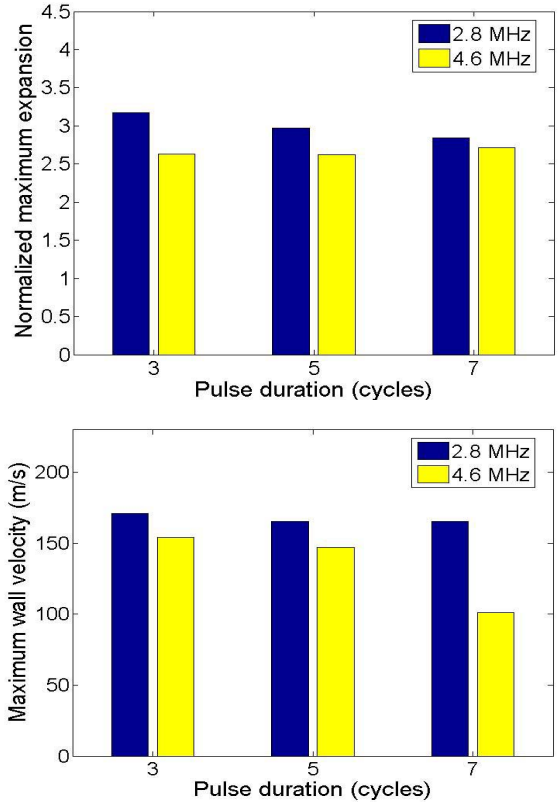


Fig 7. Maximum normalized radial expansion and peak velocity of the microbubble wall modeled using the incident pulses with peak rarefactional pressures yielding 50% destruction.

## IV. Discussion

Previous data acquired with a single PCD (13 MHz) had been difficult to interpret when a 0.9-MHz transmit frequency was applied. In effect, at 13 MHz only isolated, large bandwidth peaks were recorded allowing questions to be raised concerning the number of microbubbles in the effective volume. The form of the 0.9-MHz response recorded with the DPCD (Fig 1) is typical of the response anticipated from a single, oscillating microbubble. This oscillating behavior is outside of the 13-MHz transducer's sensitive bandwidth and only isolated, broadband emissions are detected. The post-excitation broadband signal is attributed to the IC and rebound behavior described previously. The post-excitation signals are present in both traces, demonstrating that the IC signal has very broadband content.

The normalized radial expansion at 50% destruction was between approximately 2.5 and 3 for the 2.8- and 4.6-MHz excitation. This range is consistent with that which has been proposed by several researchers [7]. The maximum wall velocities are within the 100 to 175 m/s range showing a marked decrease at 4.6 MHz when the pulse duration is increased.

## V. Conclusions

The current work extends previous estimations of minimum peak rarefactional pressure leading to a single rupture event to describe the percent rupture as a function of pressure. The 50% thresholds were on the order of 3.3 and 2 times higher than the pressures producing a single rupture event at 4.6 and 2.8 MHz, respectively. The DPCD data at 0.9-MHz excitation provide preliminary observations (peaks detected by the 13-MHz transducer during excitation associated with shape changes in the 0.9-MHz pulse-echo signal) that need to be explored further to see if there is a link between these signal features and rupturing microbubble dynamics. Comparison of the spectral response for groups of ruptured and non-ruptured bubbles demonstrates an increase in broadband noise added to spectra with otherwise similar spectral content.

The more detailed threshold information obtained in this study should be useful in selecting the pulse characteristics to apply for imaging (minimized microbubble destruction) and therapeutic (maximized microbubble destruction) applications. Comparisons between the responses (in time and frequency) of oscillating microbubbles near rupture and those that rupture at the same incident pressures provide a starting point for responding to questions concerning how much the rupture response contributes to backscattered echo.

## Acknowledgment

Authors gratefully acknowledge support from the University of Illinois at Urbana-Champaign, the Centre National de la Recherche Scientifique, France, a "Bourses de Recherche" from the Scientific Advisory Board of the Mayor of Paris and NIH Grant EB02641 (formerly HL58218), University of Illinois at Urbana-Champaign.

## References

[1] J. Eyding, W. Wilkening, M. Reckhardt, G. Schmid, S. Meves, H. Ermert, H. Przuntek, and T. Postert, "Contrast burst depletion imaging (CODIM): a new imaging procedure and analysis method for semiquantitative ultrasonic perfusion imaging," *Stroke*, vol. 34, pp. 77-83, 2003.

[2] K. Wei, A. R. Jayaweera, S. Firoozan, A. Linka, D. M. Skyba, and S. Kaul, "Quantification of myocardial blood flow with ultrasound-induced destruction of microbubbles administered as a constant venous infusion," *Circulation*, vol. 97, pp. 473-483, 1998.

[3] R. V. Shohet, S. Chen, Y. T. Zhou, Z. Wang, R. S. Meidell, R. H. Unger, and P. A. Grayburn, "Echocardiographic destruction of albumin microbubbles directs gene delivery to the myocardium," *Circulation*, vol. 101, pp. 2554-2556, 2000.

[4] J. P. Christiansen, B. A. French, A. L. Klibanov, S. Kaul, and J. R. Lindner, "Targeted tissue transfection with ultrasound destruction of plasmid-bearing cationic microbubbles," *Ultrasound Med Biol*, vol. 29, pp. 1759-1767, 2003.

[5] A. Y. Ammi, R. O. Cleveland, J. Mamou, G. I. Wang, S. L. Bridal and W. D. O'Brien, Jr, "Ultrasonic contrast agent shell rupture detected by inertial cavitation and rebound," *IEEE Trans Ultrason Ferroelectr Freq Control*, in press.

[6] S. Podell, C. Burrascano, M. Gaal, B. Golec, J. Maniquis, and P. Mehlhaff, "Physical and biochemical stability of Optison, an injectable ultrasound contrast agent," *Biotechnol Appl Biochem*, vol. 30, pp. 213-223, 1999.

[7] May, D.J., J.S. Allen, and K.W. Ferrara, *Dynamics and fragmentation of thick-shelled microbubbles.* IEEE Trans Ultrason Ferroelectr Freq Control, 2002. **49**(10): p. 1400-10.